

Critical spin fluctuations across the superconducting dome in $\text{La}_{2-x}\text{Sr}_x\text{CuO}_4$

Jacopo Radaelli,¹ Oliver J. Lipscombe,¹ Mengze Zhu,¹ J. Ross Stewart,²
Aavishkar A. Patel,³ Subir Sachdev,⁴ and Stephen M. Hayden¹

¹*H.H. Wills Physics Laboratory, University of Bristol,
Tyndall Avenue, Bristol BS8 1TL, United Kingdom*

²*ISIS Pulsed Neutron and Muon Source, Rutherford Appleton Laboratory, Didcot OX11 0QX, United Kingdom*

³*Center for Computational Quantum Physics, Flatiron Institute, 162 5th Avenue, New York, NY 10010, USA*

⁴*Department of Physics, Harvard University, Cambridge, MA 02138, USA*

Overdoped cuprate superconductors are strange metals above their superconducting transition temperature. In such materials, the electrical resistivity has a strong linear dependence on temperature (T) and electrical current is not carried by electron quasiparticles as in conventional metals. Here we demonstrate that the strange metal behavior co-exists with strongly temperature-dependent critical spin fluctuations showing dynamical scaling across the cuprate phase diagram. Our neutron scattering observations and the strange metal behavior are consistent with a spin density wave quantum phase transition in a metal with spatial disorder in the tuning parameter. Numerical computations on a Yukawa-Sachdev-Ye-Kitaev model yield an extended ‘Griffiths phase’ with scaling properties in agreement with observations, establishing that low-energy spin excitations and spatial disorder are central to the strange metal behavior.

Understanding high-temperature superconductivity in layered cuprates has posed significant challenges to the theory of condensed matter. In particular, the unusual metallic state of cuprates above their critical temperature, T_c , remains poorly understood. This state is crucial, as superconductivity emerges from it. The cuprate phase diagram is characterized by the presence of various competing orders such as antiferromagnetism (AF), charge density wave (CDW) order, and the pseudogap state in the underdoped region of the phase diagram [1]. The overdoped region is largely free from these competing phases. Nevertheless, the normal state ($T > T_c$) shows “strange metal” (SM) behavior [2] where the resistivity, ρ , is proportional to temperature, T , with a large proportionally constant. The resistivity of a metal is usually interpreted using the Drude model in which $\rho \propto \tau_{\text{tr}}^{-1}$, where τ_{tr}^{-1} is the relaxation rate of the electrons transporting current. For SMs, we find that $\tau_{\text{tr}}^{-1} \approx k_B T / \hbar$, the Planckian dissipative rate [3]. This is in stark contrast to the $\rho \propto T^2$ and $\tau_{\text{tr}}^{-1} \propto T^2$ expected to describe metals in Fermi liquid theory at low temperature. The strange behavior [4] in resistivity is accompanied by an anomalous specific heat contribution $\propto T \ln(1/T)$ in contrast to the liquid Fermi form $\propto T$.

The existence of the Planckian transport relaxation rate $\tau_{\text{tr}}^{-1}(T)$ over a wide temperature range in cuprates is challenging for theory to explain. The picture in simple metals is based on the scattering of the fermion quasiparticles near the Fermi surface off bosons (e.g. phonons). The total momentum of the system is then degraded via impurities or umklapp scattering. There are two issues with this picture with regards to cuprates [5]. First, linear or nearly-linear resistivity exists over a wide range of doping so the relevant excitations would also be present over this range. Second, the degradation of momentum mentioned above cannot be accounted for by umklapp

scattering. Thus other mechanisms are required.

Here we show that nearly-critical low-energy collective spin fluctuations are integral to the strange metal behavior in the cuprates and exist across the superconducting dome. We investigate the overdoped region a cuprate superconductor where the SM behavior is clearest [6]. The material we have chosen is $\text{La}_{2-x}\text{Sr}_x\text{CuO}_4$ (LSCO). This system can be doped over a wide range through the overdoped region of the phase diagram (Fig. 1A) and has a relatively low T_c so that the SM normal state is present over a wide range of temperature.

Spin fluctuations have been widely studied in LSCO and other cuprate superconductors by techniques such as inelastic neutron scattering, resonant inelastic x-ray scattering and nuclear magnetic resonance [11]. The parent compounds such as La_2CuO_4 are antiferromagnetic with strong super-exchange coupling J and spin wave excitations [12] up to ~ 320 meV. Upon doping these spin wave-excitations become heavily damped, with residual antiferromagnetic or spinon excitations remaining at higher energies $\gtrsim 100$ meV [7, 8] as illustrated schematically in Fig. 1B. In addition to the band of higher energy excitations, doped cuprates show low-energy excitations which are highly structured in reciprocal space [13] with the strongest excitations at $\mathbf{Q}_\delta = (1/2, 1/2 \pm \delta)$ and $(1/2 \pm \delta, 1/2)$. For underdoped compositions, with doping $x = p \sim 1/8$, these incommensurate spin fluctuations freeze for $T \lesssim T_c$ [14–16]. At higher temperatures in the normal state they are strongly temperature dependent showing the hallmarks of proximity to quantum criticality such as ω/T scaling [10, 17, 18]. For overdoped LSCO, low-energy spin fluctuations were observed to grow down to for $T \approx T_c$ [19]. For LSCO($x=0.22$) and $T \approx T_c = 26$ K it was found [20] that these excitations are described by a heavily over-damped harmonic oscillator response and have a characteristic energy scale

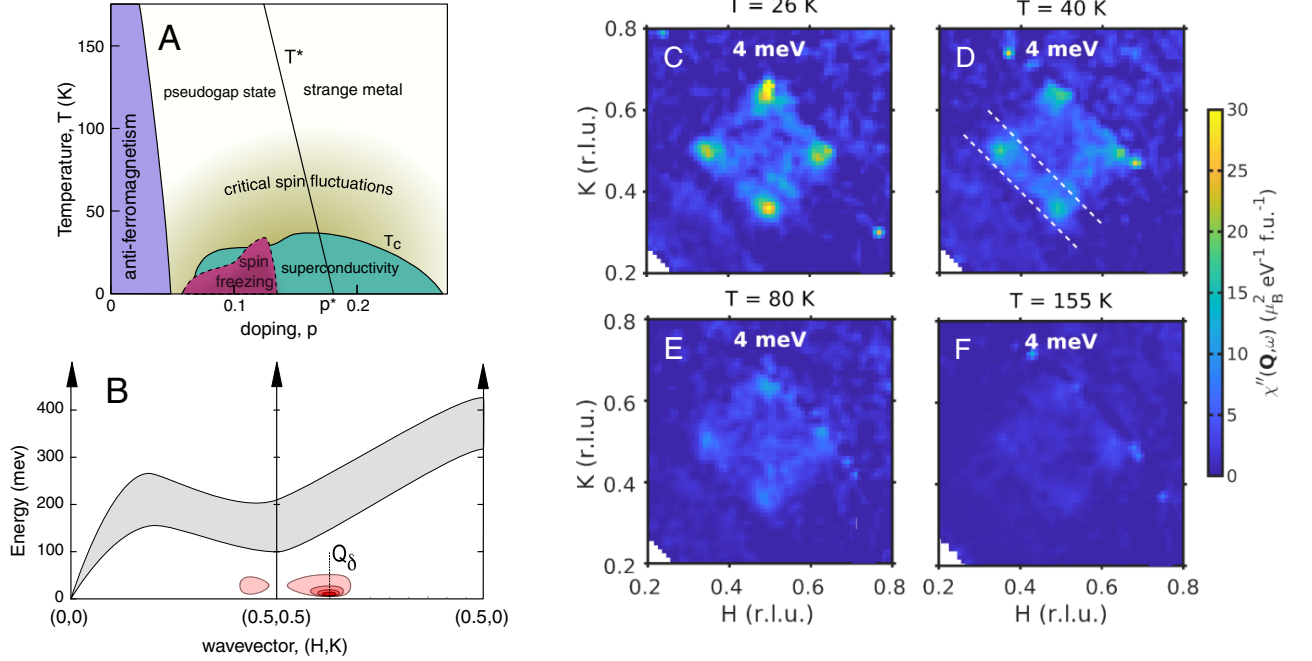


FIG. 1. **Spin fluctuations in $\text{La}_{2-x}\text{Sr}_x\text{CuO}_4$ ($x=0.22$).** (A) Schematic phase diagram of LSCO showing the critical spin fluctuations observed here. (B) Schematic of spin excitations in LSCO($x = 0.22$) based on (Refs. [7, 8]) as represented by imaginary part of the susceptibility $\chi''(\mathbf{Q}, \omega)$. Reciprocal space is labeled as $\mathbf{Q} = H\mathbf{a}^* + K\mathbf{b}^* + L\mathbf{c}^* \equiv (H, K)$. Gray region is broad high energy spin excitations [7, 8]. Pink regions are the low-energy excitations studied here. (C-F) Slices of $\chi''(\mathbf{Q}, \omega)$ for $\hbar\omega = 4$ meV, $L \in [-1, 1]$ and various temperatures (see Supplementary [9] for details). White dashed lines indicate the range over which slices are integrated to produce cuts in Fig. 2.

$$\hbar\Gamma_\delta \approx 5 \text{ meV} \approx 3k_B T.$$

We used inelastic neutron scattering to map about the \mathbf{Q} - ω dependence of the low-energy spin fluctuation in single crystals of LSCO($x= 0.22$) in the normal state for temperatures $T_c \leq T \leq 300$ K. Measurement were carried out using the LET spectrometer of the ISIS Pulsed Neutron and Muon Source [9]. Fig. 1C-F show constant energy maps of the dynamic susceptibility $\chi''(\mathbf{Q}, \omega)$ at $\hbar\omega = 4$ meV. For $T = 26$ K, the four-peaks around $\mathbf{Q} = (1/2, 1/2)$ can be clearly seen in Fig. 1C. Cuts through the peaks along the $\mathbf{Q} = (1/2 - \delta/2 + \xi, 1/2 - \delta/2 + \xi)$ line (see dashed lines in Fig. 1D) are shown in Fig. 2A. As the temperature increases, the peaks can be seen to weaken and broaden in \mathbf{Q} . The measured intensity $S(\mathbf{Q}, \omega)$ can be converted to the magnetic response function $\chi''(\mathbf{Q}, \omega)$ using the fluctuation dissipation theorem $S(\mathbf{Q}, \omega) = (1/\pi)\chi''(\mathbf{Q}, \omega)[1 - \exp(-\hbar\omega/k_B T)]^{-1}$ [9], the results shown in Fig. 2B and Fig. 3A. Our data (see Fig. 3A) show that the dynamic spin susceptibility near \mathbf{Q}_δ is strongly temperature dependent for this over-doped cuprate. The behavior is reminiscent of the approach to a quantum critical point as $T \rightarrow 0$.

At a quantum critical point, the dynamical suscepti-

bility is expected to show the scaling behavior [9, 21]

$$\chi(q, \omega) \propto T^{-\alpha} \Phi\left(\xi q, \frac{\hbar\omega}{k_B T}\right), \quad (1)$$

where $\xi \propto T^{-1/z}$ is a correlation length, z is the dynamic critical exponent, $q = |\mathbf{Q} - \mathbf{Q}_\delta|$ is wavevector relative to ordering wavevector, and Φ is a universal complex function of both arguments. For $q = 0$, the imaginary part of the dynamic susceptibility (measured here) scales [9] as

$$\chi''(q = 0, \omega) = T^{-\alpha} \phi_1\left(\frac{\hbar\omega}{k_B T}\right), \quad (2)$$

where $\alpha = \gamma/\nu z$, $\phi_1(x) = \Phi(0, x)$ is a scaling function and γ and ν are the susceptibility and correlation function temperature exponents.

In Fig. 3B we show that our data can be collapsed onto a single trend with a suitable choice of α , where $\phi_1(x)$ can be approximated by a simple Lorentzian $\phi_1(x) \propto ax/(a^2 + x^2)$ with $a = 2.9 \pm 0.3$ and $\alpha = 0.32 \pm 0.10$. This small value of α excludes the familiar paramagnon theory which has $\alpha = 1$ [22] (which also does not have an extended regime of criticality). Our data is consistent with the susceptibility having a low-frequency component

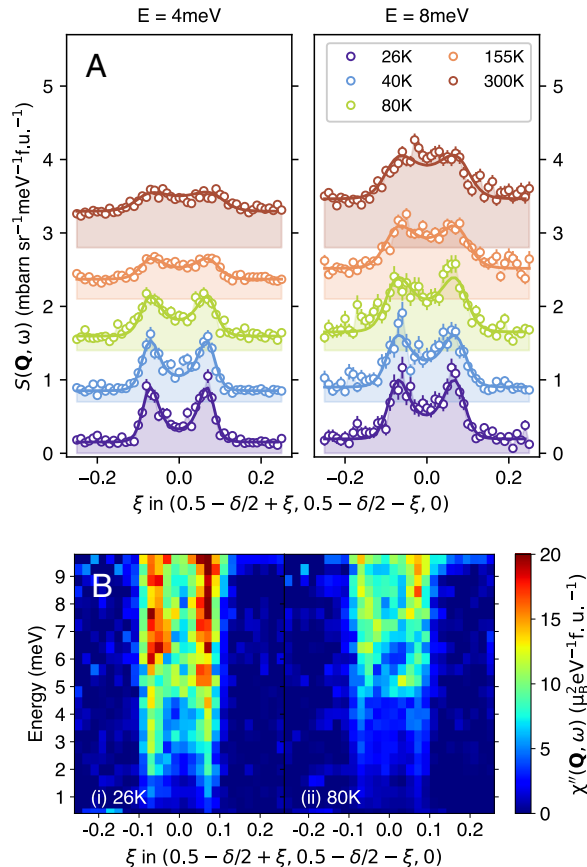


FIG. 2. **The temperature dependence to the low-energy spin fluctuations in $\text{La}_{2-x}\text{Sr}_x\text{CuO}_4$ ($x=0.22$).** (A) The scattering intensity versus wavevector \mathbf{Q} for different temperatures (bottom to top: 26, 40, 80, 155, 300 K) for energy transfers $\hbar\omega = 4, 8 \text{ meV}$. The cuts are through the incommensurate \mathbf{Q}_δ positions as shown by the dashed lines in Fig. 1D. (B) $E - \mathbf{Q}$ map of the magnetic response function $\chi''(\mathbf{Q}, \omega)$ for $T = 26, 80 \text{ K}$ showing its evolution with temperature. The trajectory of \mathbf{Q} is the same as that in (A).

that varies as

$$\chi''(\mathbf{Q}_\delta, \omega) = \frac{\chi'(\mathbf{Q}_\delta)\Gamma_\delta \omega}{\Gamma_\delta^2 + \omega^2}, \quad (3)$$

where the real part of the susceptibility $\chi'(\mathbf{Q}_\delta) \propto T^{-\alpha}$ and spin relaxation rate varies as

$$\hbar\Gamma_\delta = ak_B T, \quad (4)$$

as shown inset of Fig. 3A. Thus our data is consistent with Γ_δ tracking the Planckian relaxation rate $\tau_{\text{tr}}^{-1} \propto T$ as observed in transport measurements suggesting that they are related.

We can gain more information about the criticality of the spin fluctuations from the \mathbf{Q} -dependence of $\chi''(\mathbf{Q}, \omega)$. From Eqn. 3 we see that $\chi''(q, \omega) \propto \omega$ as $\omega \rightarrow 0$ so there

will be peaks in $\chi''(\mathbf{Q}, \omega)/\omega$ at the lowest energies. It can be shown from the scaling of the susceptibility [9] that

$$\left. \frac{\chi''(q, \omega)}{\omega} \right|_{\omega \rightarrow 0} \propto T^{-(\alpha+1)} \phi_2(\xi q). \quad (5)$$

The function $\phi_2(\xi q)$ is peaked at the ordering wavevector $q = 0$ with width ξ^{-1} . We can determine z from the temperature dependence of ξ^{-1} .

In order to fit our data, we use a form previously used [10, 20] to describe the low-energy response of the cuprates:

$$\chi''(\mathbf{Q}, \omega) = \chi''(\mathbf{Q}_\delta, \omega) \frac{\kappa^4(\omega)}{[\kappa^2(\omega) + R(\mathbf{Q})]^2}, \quad (6)$$

where $R(\mathbf{Q})$ is a function with zeros at the \mathbf{Q}_δ positions and the property $R(\mathbf{Q}_\delta) = |\mathbf{q}|^2$ for $\mathbf{q} \rightarrow 0$, the second factor represents $\phi_2(\xi q)$ in the limit $\omega \rightarrow 0$ and we can make the association $\kappa(\omega = 0) \equiv \xi^{-1}$ [9]. Example fits to Eqn. 6 are shown in Fig. 2. The resulting fitted values of $\kappa(\omega)$ (\mathbf{Q} -width of response) are shown in Fig. 3D,E,F. In Fig. 3D we see that $\kappa(\omega)$ increases with ω and T . We posit that the effects of ω and T add in quadrature and this suggests the form

$$\kappa^2(\omega) \propto (\hbar\omega)^{2/z} + r(k_B T)^{2/z}, \quad (7)$$

where $\kappa(\omega = 0) = \xi^{-1} \propto T^{1/z}$ and r is the ratio of the temperature and energy contributions which we set equal to one. We find that Eqn. 7 can be used to collapse the experimentally determined $\kappa(\omega, T)$ onto a single solid line as shown in Fig. 3E,F with $z = 1.83 \pm 0.35$. In the Supplementary [9] we show that our data are also consistent with the system being tuned slightly away from quantum criticality (dashed line in Fig. 3F).

Here we only study the normal state, however, we can extrapolate the data to lower temperatures. Fig. 3 suggests that the spin fluctuations would continue to evolve as $T \rightarrow 0$ in the absence of superconductivity. This is supported by measurements made where superconductivity is suppressed by magnetic field. Neutron scattering measurements [20] show that Γ_δ continues to decrease below T_c when a 9 Tesla field is applied. High field ($B \gtrsim B_{c2}$) heat capacity measurements show a $\sim T \log(1/T)$ contribution [23] and, resistivity measurements in a high field [6] show a $\rho \propto T$ behavior as $T \rightarrow 0$.

Thus we have found that the low-energy spin fluctuations of the overdoped superconductor LSCO ($x = 0.22$) show the hallmarks of quantum criticality. Specifically, we observe ω/T scaling and a dynamical critical exponent $z = 1.83 \pm 0.35$. Our value of z for LSCO ($x = 0.22$) is consistent with the $z = 2$ value expected [24] for a 2D antiferromagnetic metal at a QCP with coupling between electrons and spin fluctuations. It is important to view this result in the context of the whole cuprate phase diagram. Previous T -dependent measurements in

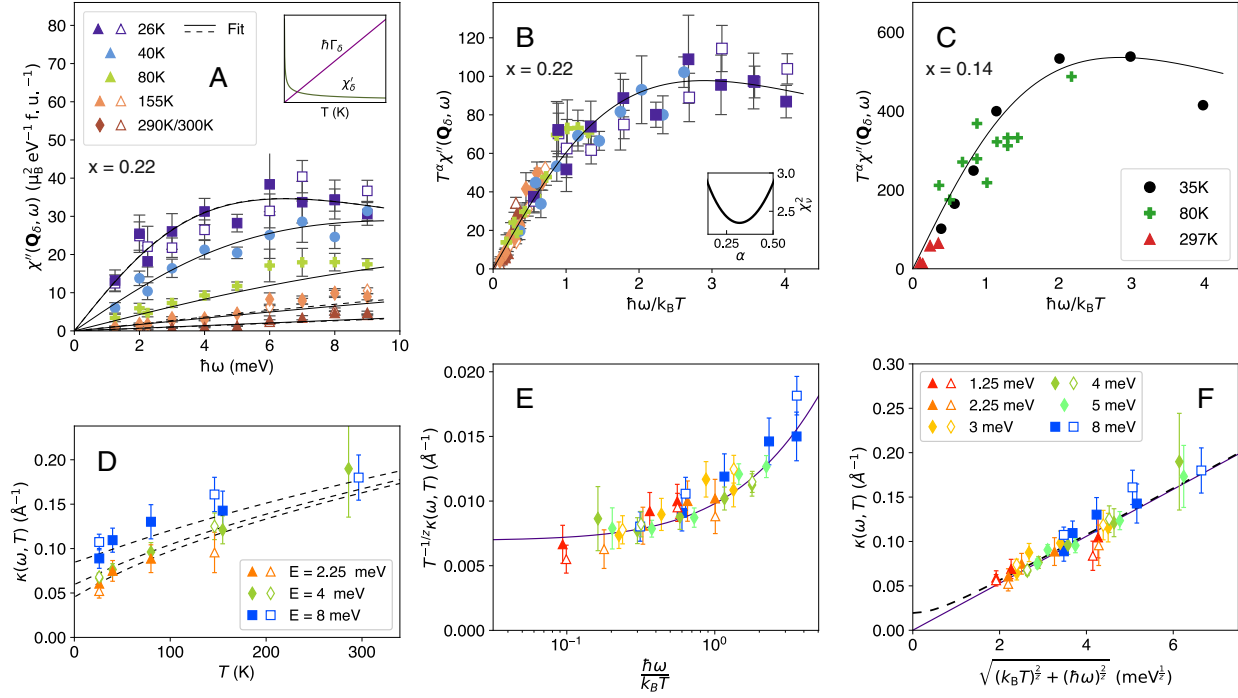


FIG. 3. **Scaling behavior of the dynamic magnetic susceptibility and correlation length in $\text{La}_{2-x}\text{Sr}_x\text{CuO}_4$** (A) Temperature dependence of $\chi''(\mathbf{Q}, \omega)$ at ordering wavevector \mathbf{Q}_δ . Lines are fits to Eqn. 3. Inset shows the T -dependence of the spin relaxation rate Γ_δ and real part of the susceptibility $\chi'(\mathbf{Q}_\delta)$ obtained when data are modeled with Eqns. 3-4. (B) ω/T scaling plot of the $x = 0.22$ data in (A) using Eqn. 2 and the procedure described in [9]. The inset shows how the quality of the collapse [9] varies with exponent α . (C) Scaling plot for underdoped LSCO $x = 0.14$ data from Ref. [10]. This data shows a similar collapse to the $x = 0.22$ data in (B). (D) The width in \mathbf{Q} of $\chi''(\mathbf{Q}, \omega)$ is denoted by the inverse dynamic correlation length $\kappa(\omega)$. Here we plot $\kappa(\omega)$ versus temperature for $\hbar\omega = 1.25, 2.25, 4, 8$ meV. (E) Data in (D) can be collapsed onto a single trend line with suitable choice of z and ω/T scaling. (F) Data in (D) can be scaled onto a single line using (7) allowing the dynamic critical exponent z to be determined. Dashed line is Eqn. S15 [9].

the normal state of underdoped LSCO ($x = 0.14$) [10] show a related ω/T scaling when replotted and analyzed in same way as the present data. LSCO ($x = 0.14$) shows a smaller dynamical critical exponent $z \approx 1$, suggesting that z increases with doping. Combining the results of the two studies we conclude that the normal state hosts low-energy critical fluctuations across the phase diagram as illustrated in Fig. 1A.

We now discuss our results in the context of the p - T phase diagram (Fig. 1A). A region of glassy spin-freezing is observed [14–16, 25] near $p \approx 1/8$ (also seen in other cuprates [26]). This region appears to be connected to charge ordering is present in other cuprates [26] and can be expanded by the application of a large magnetic field [15, 16, 25]. Inside this region T -linear resistivity is not observed [16]. For larger dopings i.e. $p \gtrsim 0.14$ there is a region where ω/T scaling in $\chi''(\mathbf{Q}_\delta, \omega)$ and approximately T -linear behavior in the resistivity [6] co-exist in the absence of spin-freezing.

Understanding the strange metal behavior seen in LSCO and other cuprates is one of the major challenges in condensed matter physics. It occurs across a diverse set of materials that include transition metal oxides, heavy fermions [27, 28], iron-based superconductors [2, 4]. Planckian dissipation provides a universal phenomenology representing a quantum limit on the current-carrying degrees of freedom of a metal [3]. However, it does not indicate a microscopic mechanism. The behavior in the resistivity has often been associated with an underlying magnetic quantum critical point (QCP) at $T = 0$. In a typical scenario the system is tuned to the QCP and strange metal behaviour is observed over a relatively small range of parameter space. This is observed in some systems such as $\text{Sr}_3\text{Ru}_2\text{O}_7$ [29, 30]. However, there are many examples including not only cuprates but twisted-layer graphene and twisted transitional-metal dichalcogenides where it persists over of an extended region. Extended critical be-

haviour has also been observed in MnSi with $\rho \propto T^{3/2}$.

In recent years new insights have been gained by considering the Hertz-Millis theory [24, 33] for the onset of magnetic order in metals, but in the presence of spatial disorder in the tuning parameter. Such physics can be described by Yukawa-Sachdev-Ye-Kitaev models [5, 31, 32, 34, 35], as discussed in the Supplementary [9]. In particular, it has been shown that the inclusion of disorder can explain the existence of the SM-behavior down to the lowest temperatures and over an extended range of doping. Applying this general picture to the cuprates it is postulated that disorder delays the onset of long range spin order giving rise to a “quantum Griffiths phase” [31, 32, 36] (similar to that in the two-dimensional Ising model in a transverse field [37]) as a transition tuning parameter λ is reduced. SM linear- T resistivity is observed over an extended range of λ that comprises part of the Griffiths phase instead of QCP. The tuning parameter λ is controlled by the doping x . The inclusion of disorder is logical in the $\text{La}_{2-x}\text{Sr}_x\text{CuO}_4$ system because of the perturbation caused by Sr doping in the plane neighboring the CuO_2 plane.

Returning to the strange metal behavior in the resistivity observed in LSCO and other cuprates. An extended Drude analysis of optical conductivity $\sigma(\omega)$ of cuprates shows that the optical scattering rate $\tau_{\text{op}}^{-1}(\omega)$ is strongly frequency dependent [38, 39] indicating the current carrying electrons are scattered inelastically. This is incompatible with elastic scattering from impurities or defects. Phonon scattering cannot produce the T -linear resistivity at low temperature below the Debye temperature scales. This has led some to conclude that disorder in strange metals must scatter electrons inelastically [5, 35]. The optical scattering rate $\tau_{\text{op}}^{-1}(\omega)$ provides a further insight into the nature of strange metals as it found to show ω/T scaling over a wide range of ω/T [39].

In Fig. 4 we show numerical calculations of the critical spin susceptibility $\chi''(\mathbf{Q}_\delta, \omega)$ from a Yukawa-Sachdev-Ye-Kitaev model [9]. An approximate method [31] allows exact analytic continuation to real frequency, while imaginary time quantum Monte Carlo studies [32] yield precise values of exponents. The form (6) is an excellent fit to the theory [9], and this allows determination of $\kappa(\omega, T)$, which is also shown. The results have been scaled in the same way as Fig. 3B,E and we find excellent real frequency scaling at the quantum critical value of the tuning parameter $\lambda = \lambda_c = -0.4586$ with $\alpha = 0.84$ and $z = 2.13$. Corresponding scaling plots within the quantum Griffiths phase, $\lambda > \lambda_c$ appear in the Supplementary [9]: the ω/T scaling is still present, but it is better at smaller values of ω/T , and for the local spin susceptibility. The better scaling of the local susceptibility is as expected from the localized nature of the spin fluctuations in the Griffiths region. The value of the exponent α decreases significantly with increasing λ , down to $\alpha \approx 0.5$ at $\lambda = -0.43$.

A separate, and in principle, exact determination of α is obtained from the imaginary frequency susceptibility (Ω_m) of the quantum Monte results of Ref. [32] (Fig. 4E). This also obeys Ω_m/T scaling and yields $\alpha \approx 0.2$ in the Griffiths region, compatible with the our observations at $x = 0.22$. We note that ω/T scaling fails in our theory at very low T [9], as it does in the Ising model in a transverse field [37], presumably due to the dominance of rare regions: future observations at even lower T are therefore of interest.

The same theory is able to produce a linear resistivity and Planckian behavior in the transport and optical scattering rates [31] yielding a consistent picture of the strange metal, as shown in Fig. 4F, with similar results at other values of λ in the Supplementary [9]. There is linear-in- T behavior, but with different slopes at lower and higher T : we can identify these with the ‘foot’ and ‘fan’ regimes, associated with Griffiths and marginal Fermi liquid behaviors respectively [6, 39, 40]. The low T upturn in Fig. 4C in κ for $\omega > T$ is possibly also related to the crossover between these ‘foot’ and ‘fan’ regimes.

In summary, we have observed critical spin fluctuations with ω/T scaling in an overdoped cuprate superconductor. When combined with earlier measurements [10] this shows that there is an extended region of critical spin-fluctuations in $\text{La}_{2-x}\text{Sr}_x\text{CuO}_4$. We have compared our observations with numerical studies of a Yukawa-Sachdev-Ye-Kitaev model for the onset of spin density wave order in a disordered metal and found good agreement. Both experiment and theory/numerics find an extended ‘Griffiths’ phase of both ω/T magnetic susceptibility scaling and T -linear resistivity. Such scaling is present even though there is no criticality in the usual sense of a diverging correlation length [9]. The correlation length diverges at the lower doping boundary of the Griffiths region, and the large correlation length allows definition of a finite dynamic exponent z which is doping (tuning parameter) dependent. The spin excitations show $z \approx 2$, or larger, and are consistent with contribution with spin relaxation rate $\hbar\Gamma_\delta \approx 3k_B T$. The observations may be related to singular charge density fluctuations observed in EELS [41]. The strongly T -dependent spin fluctuations coexist with transport properties described by Planckian dissipation, showing the spin degrees of freedom in the presence of spatial disorder are at the heart of strange metal behavior. It would be interesting to study the role of such critical spin fluctuations in high temperature d -wave superconductivity [42].

S.M.H is grateful to Jörg Schmalian for sharing insights about scaling theory. A.A.P. and S.S. thank Peter Lunts for related collaborations. Neutron beamtime was provided by the ISIS neutron and muon source through proposals RB2220248 and RB2410260. The Flatiron Institute is a division of the Simons Foundation. S.S. was supported by the U.S. National Science Foundation grant No. DMR-2245246.

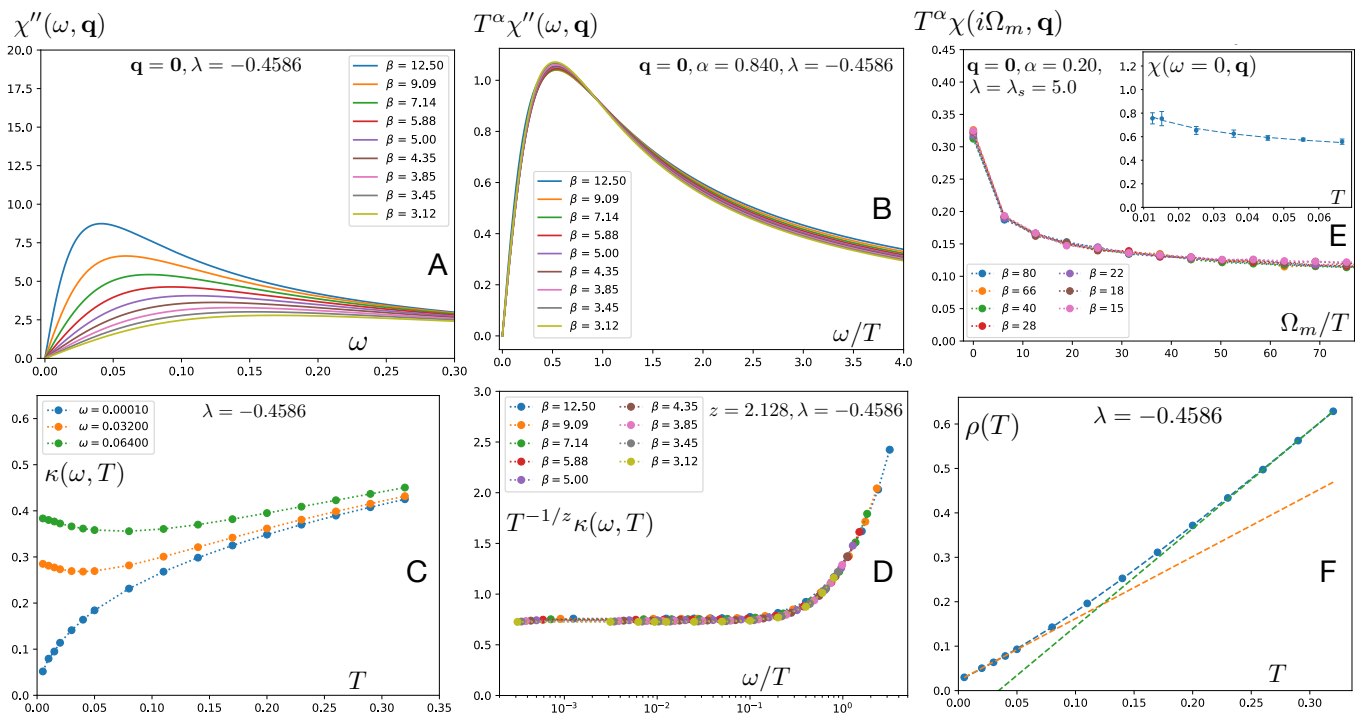


FIG. 4. **Numerical theoretical results for low energy spin fluctuations.** (A-D) Compare with the experimental plots in Fig. 3A,B,D,E ($\beta = 1/T$). Obtained from the results of Ref. [31] (with a mean-field treatment of interactions, but exact treatment of disorder), at the critical value of $\lambda = \lambda_c = -0.4586$, after exact analytic continuation to real frequencies [9]; results for $\lambda > \lambda_c$, and parameter values are in the Supplementary [9], where we also estimate ≈ 33 meV as the unit of energy/frequency/temperature in the numerics. (A-B) Dynamic spin susceptibility and its scaling plot, with best-fit exponent $\alpha = 0.84$. (C-D) Inverse correlation length κ and its scaling plot, with best-fit exponent $z = 2.128$. (E) Computations of imaginary frequency (Ω_m) susceptibility by (in principle, exact) quantum Monte Carlo results for the YSYK model in Ref. [32], at the end of the strange metal phase that is present for $\lambda_s = 5.0 \leq \lambda \leq \lambda_G = 5.5$. The dashed line in the inset is a fit to $\sim T^\alpha$. Both plots yield $\alpha = 0.20$. (F) **Resistivity from spin fluctuations.** Computed from the spin susceptibility, as described in Ref. [31]. Note the distinct slopes of linear-in- T resistivity at low and high T .

-
- [1] B. Keimer, S. A. Kivelson, M. R. Norman, S. Uchida, and J. Zaanen, *Nature* **518**, 179 (2015).
- [2] P. W. Phillips, N. E. Hussey, and P. Abbamonte, *Science* **377**, eabh4273 (2023).
- [3] J. Zaanen, *Nature* **430**, 512 (2004).
- [4] S. A. Hartnoll and A. P. Mackenzie, *Rev. Mod. Phys.* **94**, 041002 (2022).
- [5] A. A. Patel, H. Guo, I. Esterlis, and S. Sachdev, *Science* **381**, 790 (2023).
- [6] R. A. Cooper, Y. Wang, B. Vignolle, O. J. Lipscombe, S. M. Hayden, Y. Tanabe, T. Adachi, Y. Koike, M. Nohara, H. Takagi, C. Proust, and N. E. Hussey, *Science* **323**, 603 (2009).
- [7] O. J. Lipscombe, S. M. Hayden, B. Vignolle, D. F. McMorrow, and T. G. Perring, *Phys. Rev. Lett.* **99**, 067002 (2007).
- [8] H. C. Robarts, M. Barthélemy, K. Kummer, M. García-Fernández, J. Li, A. Nag, A. C. Walters, K. J. Zhou, and S. M. Hayden, *Phys. Rev. B* **100**, 214510 (2019).
- [9] See Supplemental Material, which includes Refs. [43–49], for additional discussion and more theoretical results.
- [10] G. Aeppli, T. Mason, S. Hayden, H. Mook, and J. Kulda, *Science* **278**, 1432 (1997).
- [11] M. Fujita, H. Hiraka, M. Matsuda, M. Matsuura, J. M. Tranquada, S. Wakimoto, G. Xu, and K. Yamada, *J. Phys. Soc. Jpn.* **81**, 011007 (2011).
- [12] N. S. Headings, S. M. Hayden, R. Coldea, and T. G. Perring, *Phys. Rev. Lett.* **105**, 247001 (2010).
- [13] S. W. Cheong, G. Aeppli, T. E. Mason, H. Mook, S. M. Hayden, P. C. Canfield, Z. Fisk, K. N. Clausen, and J. L. Martinez, *Phys. Rev. Lett.* **67**, 1791 (1991).
- [14] T. Suzuki, T. Goto, K. Chiba, T. Shinoda, T. Fukase, H. Kimura, K. Yamada, M. Ohashi, and Y. Yamaguchi, *Phys. Rev. B* **57**, R3229 (1998).
- [15] M. Frachet, I. Vinograd, R. Zhou, S. Benhabib, S. Wu, H. Mayaffre, S. Krämer, S. K. Ramakrishna, A. P. Reyes, J. Debray, T. Kurosawa, N. Momono, M. Oda, S. Komiya, S. Ono, M. Horio, J. Chang, C. Proust, D. LeBoeuf, and M.-H. Julien, *Nature Physics* **16**, 1064 (2020).
- [16] D. J. Campbell, M. Frachet, V. Oliviero, T. Kurosawa, N. Momono, M. Oda, J. Chang, D. Vignolles, C. Proust, and D. LeBoeuf, “Strange metal from spin fluctuations in a cuprate superconductor,” (2024), arXiv:2412.03720 [cond-mat.supr-con].
- [17] S. M. Hayden, G. Aeppli, H. Mook, D. Rytz, M. F. Hundley, and Z. Fisk, *Phys. Rev. Lett.* **66**, 821 (1991).

- [18] B. Keimer, R. J. Birgeneau, A. Cassanho, Y. Endoh, R. W. Erwin, M. A. Kastner, and G. Shirane, *Phys. Rev. Lett.* **67**, 1930 (1991).
- [19] S. Wakimoto, H. Zhang, K. Yamada, I. Swainson, H. Kim, and R. J. Birgeneau, *Phys. Rev. Lett.* **92**, 217004 (2004).
- [20] M. Zhu, D. J. Voneshen, S. Raymond, O. J. Lipscombe, C. C. Tam, and S. M. Hayden, *Nat. Phys.* **19**, 99 (2023).
- [21] S. Sachdev and J. Ye, *Phys. Rev. Lett.* **69**, 2411 (1992).
- [22] A. J. Millis, H. Monien, and D. Pines, *Phys. Rev. B* **42**, 167 (1990).
- [23] C. Girod, D. LeBoeuf, A. Demuer, G. Seyfarth, S. Imajo, K. Kindo, Y. Kohama, M. Lizaire, A. Legros, A. Gourgout, H. Takagi, T. Kurosawa, M. Oda, N. Momono, J. Chang, S. Ono, G.-q. Zheng, C. Marcenat, L. Taillefer, and T. Klein, *Phys. Rev. B* **103**, 214506 (2021).
- [24] A. J. Millis, *Phys. Rev. B* **48**, 7183 (1993).
- [25] J. Chang, C. Niedermayer, R. Gilardi, N. B. Christensen, H. M. Rønnow, D. F. McMorrow, M. Ay, J. Stahn, O. Sobolev, A. Hiess, S. Pailhes, C. Baines, N. Momono, M. Oda, M. Ido, and J. Mesot, *Phys. Rev. B* **78**, 104525 (2008).
- [26] T. Wu, H. Mayaffre, S. Krämer, M. Horvatić, C. Berthier, C. T. Lin, D. Haug, T. Loew, V. Hinkov, B. Keimer, and M.-H. Julien, *Phys. Rev. B* **88**, 014511 (2013).
- [27] M. C. Aronson, R. Osborn, R. A. Robinson, J. W. Lynn, R. Chau, C. L. Seaman, and M. B. Maple, *Phys. Rev. Lett.* **75**, 725 (1995).
- [28] W. J. Gannon, L. S. Wu, I. A. Zaliznyak, W. H. Xu, A. M. Tsvelik, Y. Qiu, J. A. Rodriguez-Rivera, and M. C. Aronson, *Proceedings of the National Academy of Science* **115**, 6995 (2018), arXiv:1712.04033 [cond-mat.str-el].
- [29] J. A. N. Bruin, H. Sakai, R. S. Perry, and A. P. Mackenzie, *Science* **339**, 804 (2013).
- [30] C. Lester, S. Ramos, R. S. Perry, T. P. Croft, M. Laver, R. I. Bewley, T. Guidi, A. Hiess, A. Wildes, E. M. Forgan, and S. M. Hayden, *Nat. Commun.* **12**, 5798 (2021).
- [31] A. A. Patel, P. Lunts, and S. Sachdev, *Proceedings of the National Academy of Sciences* **121**, e2402052121 (2024).
- [32] A. A. Patel, P. Lunts, and M. S. Albergo, “Strange metals and planckian transport in a gapless phase from spatially random interactions,” (2024), arXiv:2410.05365 [cond-mat.str-el].
- [33] J. A. Hertz, *Phys. Rev. B* **14**, 1165 (1976).
- [34] I. Esterlis, H. Guo, A. A. Patel, and S. Sachdev, *Phys. Rev. B* **103**, 235129 (2021).
- [35] C. Li, D. Valentinis, A. A. Patel, H. Guo, J. Schmalian, S. Sachdev, and I. Esterlis, *Phys. Rev. Lett.* **133**, 186502 (2024).
- [36] J. A. Hoyos, C. Kotabage, and T. Vojta, *Phys. Rev. Lett.* **99**, 230601 (2007).
- [37] O. Motrunich, S.-C. Mau, D. A. Huse, and D. S. Fisher, *Phys. Rev. B* **61**, 1160 (2000).
- [38] J. P. Carbotte, T. Timusk, and J. Hwang, *Reports on Progress in Physics* **74**, 066501 (2011).
- [39] B. Michon, C. Berthod, C. W. Rischau, A. Ataei, L. Chen, S. Komiya, S. Ono, L. Taillefer, D. van der Marel, and A. Georges, *Nature Communications* **14**, 3033 (2023).
- [40] S. Sachdev, “The foot, the fan, and the cuprate phase diagram: Fermi-volume-changing quantum phase transitions,” (2025), arXiv:2501.16417 [cond-mat.str-el].
- [41] X. Guo, J. Chen, F. Hoveyda-Marashi, S. L. Bettler, D. Chaudhuri, C. S. Kengle, J. A. Schneeloch, R. Zhang, G. Gu, T.-C. Chiang, A. M. Tsvelik, T. Faulkner, P. W. Phillips, and P. Abbamonte, “Conformally invariant charge fluctuations in a strange metal,” (2024), arXiv:2411.11164 [cond-mat.str-el].
- [42] A. Abanov, A. V. Chubukov, and A. M. Finkel’stein, *Europhys. Lett.* **54**, 488 (2001).
- [43] P. A. Lee and T. V. Ramakrishnan, *Rev. Mod. Phys.* **57**, 287 (1985).
- [44] J. H. Van Vleck, *Rev. Mod. Phys.* **34**, 681 (1962).
- [45] T. Vojta, C. Kotabage, and J. A. Hoyos, *Phys. Rev. B* **79**, 024401 (2009).
- [46] T. Vojta, in *Lectures on the Physics of Strongly Correlated Systems XVII: Seventeenth Training Course in the Physics of Strongly Correlated Systems*, American Institute of Physics Conference Series, Vol. 1550, edited by A. Avella and F. Mancini (AIP, 2013) pp. 188–247, arXiv:1301.7746 [cond-mat.dis-nn].
- [47] A. Del Maestro, B. Rosenow, M. Müller, and S. Sachdev, *Phys. Rev. Lett.* **101**, 035701 (2008).
- [48] S. M. Hayden, G. Aeppli, R. Osborn, A. D. Taylor, T. G. Perring, S. W. Cheong, and Z. Fisk, *Phys. Rev. Lett.* **67**, 3622 (1991).
- [49] R. Ewings, A. Buts, M. Le, J. van Duijn, I. Bustinduy, and T. Perring, *Nuclear Instruments and Methods in Physics Research Section A: Accelerators, Spectrometers, Detectors and Associated Equipment* **834**, 132 (2016).

Supplementary Materials for Critical spin fluctuations across the superconducting dome in $\text{La}_{2-x}\text{Sr}_x\text{CuO}_4$

Jacopo Radaelli,¹ Oliver J. Lipscombe,¹ Mengze Zhu,¹ J. Ross Stewart,²
Aavishkar A. Patel,³ Subir Sachdev,⁴ and Stephen M. Hayden¹

¹*H.H. Wills Physics Laboratory, University of Bristol,
Tyndall Avenue, Bristol BS8 1TL, United Kingdom*

²*ISIS Pulsed Neutron and Muon Source, Rutherford Appleton Laboratory, Didcot OX11 0QX, United Kingdom*

³*Center for Computational Quantum Physics, Flatiron Institute, 162 5th Avenue, New York, NY 10010, USA*

⁴*Department of Physics, Harvard University, Cambridge, MA 02138, USA*

THEORY

Dynamic critical scaling

The dynamic susceptibility of systems below their upper critical dimension is expected to obey the following scaling behavior:

$$\chi(q, \omega, T, t) = b^{\gamma/\nu} \chi(bq, b^z \omega, b^z T, b^{1/\nu} t), \quad (\text{S1})$$

where b is an arbitrary scaling parameter, t is a tuning control parameter [$t = 0$ corresponds to the quantum critical point (QCP)], q is momentum relative to ordering wavevector, γ and ν are the usual susceptibility and correlation function exponents. That is $\chi \propto t^{-\gamma}$ and $\xi \propto t^{-\nu}$. We expect the usual scaling relationship $\gamma = (2 - \eta)\nu$.

Dynamic scaling at the ordering wavevector and QCP. We suppose to be at the QCP ($t = 0$) and consider the ordering wavevector ($q = 0$). For the imaginary part of susceptibility we have

$$\chi''(q = 0, \omega, T) = \chi''(q = 0, \omega, T, t = 0) \quad (\text{S2})$$

$$= b^{\gamma/\nu} \chi''(q = 0, b^z \omega, b^z T), \quad (\text{S3})$$

since b is arbitrary, we can choose $b^z T = 1$, $b = T^{-1/z}$. It then follows that

$$\chi''(q = 0, \omega, T) = T^{-\frac{\gamma}{\nu z}} \phi_1\left(\frac{\omega}{T}\right), \quad (\text{S4})$$

$\phi_1(x)$ is a scaling function and we can collapse data onto a single trend with a suitable choice of $\frac{\gamma}{\nu z}$.

From Eqn. S1, we have for $t = 0$,

$$\chi(q, \omega, T) = b^{\gamma/\nu} \chi(bq, b^z \omega, b^z T). \quad (\text{S5})$$

Assuming a linear susceptibility near $\omega = 0$, the low-frequency slope is:

$$\left. \frac{\chi''(q, \omega, T)}{\omega} \right|_{\omega \rightarrow 0} = b^{\gamma/\nu} b^z \left. \frac{\chi''(bq, b^z \omega, b^z T)}{b^z \omega} \right|_{b^z \omega \rightarrow 0}. \quad (\text{S6})$$

Again using $b^z T = 1$,

$$\left. \frac{\chi''(q, \omega, T)}{\omega} \right|_{\omega \rightarrow 0} = T^{-\left(\frac{\gamma}{\nu z} + 1\right)} \left. \frac{\chi''(T^{-\frac{1}{z}} q, \omega, 1)}{\omega} \right|_{\omega \rightarrow 0}, \quad (\text{S7})$$

$$= T^{-\left(\frac{\gamma}{\nu z} + 1\right)} \phi_2(T^{-\frac{1}{z}} q) \quad (\text{S8})$$

where

$$\phi_2(x) = \left. \frac{\chi''(x, \omega, 1)}{\omega} \right|_{\omega \rightarrow 0}. \quad (\text{S9})$$

$$(\text{S10})$$

If $\phi_2(x)$ is a function peaked at the ordering wavevector $q = 0$ with width w . We can determine z from the temperature dependence of the width

$$w = \xi^{-1} \propto T^{\frac{1}{z}}. \quad (\text{S11})$$

Phenomenological susceptibility for spin fluctuations

We parameterize our normal-state data with a phenomenological susceptibility used by Aeppli *et al.* [1] :

$$\chi''(\mathbf{Q}, \omega) = \chi''(\mathbf{Q}_\delta, \omega) \frac{\kappa^4(\omega)}{[\kappa^2(\omega) + R(\mathbf{Q})]^2}, \quad (\text{S12})$$

where

$$R(\mathbf{Q}) = \frac{1}{4\delta^2} \left\{ \left[\left(H - \frac{1}{2} \right)^2 + \left(K - \frac{1}{2} \right)^2 - \delta^2 \right]^2 + 4 \left(H - \frac{1}{2} \right)^2 \left(K - \frac{1}{2} \right)^2 \right\}. \quad (\text{S13})$$

$R(\mathbf{Q})$ has zeros at the positions $\mathbf{Q}_\delta = (1/2 \pm \delta, 1/2)$ and $(1/2 \pm \delta, 1/2)$ and this function approximately reproduces the \mathbf{Q} dependence of our data. Near each \mathbf{Q}_δ , $R(\mathbf{Q}_\delta + \mathbf{q}) = |\mathbf{q}|^2$. Therefore,

$$\lim_{|\mathbf{q}| \rightarrow 0} \chi''(\mathbf{Q}, \omega) = \frac{\chi''(\mathbf{Q}_\delta, \omega)}{[1 + \kappa^{-2}(\omega) |\mathbf{q}|^2]^2} \quad (\text{S14})$$

and we can interpret $\kappa^{-1}(\omega)$ as a “dynamic correlation length” with usual static correlation length given by $\xi = \kappa^{-1}(\omega)$.

$\kappa(\omega, T)$ model

$$\kappa^2(\omega) = \Delta + a_0^{-2} \left[\left(\frac{\hbar\omega}{E_\kappa} \right)^{2/z} + r \left(\frac{k_B T}{E_\kappa} \right)^{2/z} \right] \quad (\text{S15})$$

We fit $\kappa(\omega, T)$ in units of \AA^{-1} to the model in Eqn. S15 fixing r to be 1 as has been found to be approximately true in LSCO $x=0.14$ [1]. Here Δ is a tuning parameter which is zero for a QCP, E_κ is an energy scale and a_0 is the in-plane lattice parameter. This fit gives $z = 1.83 \pm 0.35$, $\Delta = (4 \pm 14) \times 10^{-4} \text{\AA}^{-2}$ and $E_\kappa = 68 \pm 17 \text{ meV}$. Thus Δ is zero within the resolution of the experiment.

Quantum phase transitions in metals with Harris disorder

This section recalls the theoretical model presented in Ref. [2], and describes the computation of its real frequency response functions. There is some overlap of the initial discussion here with the review in Ref. [3].

We focus on quantum fluctuations of the spin density wave (SDW) order parameter across the quantum phase transition from the Fermi liquid [4, 5]. We write the SDW order as ($a = x, y, z$)

$$S_a(\mathbf{r}) = \sum_{\ell} \phi_{\ell a} e^{i\mathbf{Q}_{\delta\ell} \cdot \mathbf{r}} \quad (\text{S16})$$

where S_a is the electron spin at position \mathbf{r} , $\ell = 1 \dots 4$ labels the 4 ordering wavevectors (fix this) $\mathbf{Q}_{\delta\ell}$ at $(1/2, 1/2 \pm \delta)$ and $(1/2 \pm \delta, 1/2)$. We are interested in fluctuations of the SDW order parameters $\phi_{\ell a}$ coupled to electrons $c_{\mathbf{k}\sigma}$ with dispersion $\varepsilon(\mathbf{k})$ which has a Fermi surface. Including the effects of spatial disorder, we have a two-dimensional Yukawa-Sachdev-Ye-Kitev model with the imaginary time (τ) Lagrangian [6, 7]

$$\begin{aligned} \mathcal{L}_{YSYK} = & \sum_{\mathbf{k}} c_{\mathbf{k}\sigma}^\dagger \left(\frac{\partial}{\partial \tau} + \varepsilon(\mathbf{k}) \right) c_{\mathbf{k}\sigma} + \int d^2\mathbf{r} \left\{ \lambda [\phi(\mathbf{r})]^2 \right. \\ & + [g + g'(\mathbf{r})] \sum_{\ell} c_{\sigma}^\dagger(\mathbf{r}) \tau_{\sigma\sigma'}^a c_{\sigma'}(\mathbf{r}) \phi_{\ell a}(\mathbf{r}) e^{i\mathbf{Q}_{\delta\ell} \cdot \mathbf{r}} \quad (\text{S17}) \\ & \left. + K [\nabla_{\mathbf{r}} \phi(\mathbf{r})]^2 + u [\phi(\mathbf{r})]^4 + v(\mathbf{r}) c_{\sigma}^\dagger(\mathbf{r}) c_{\sigma}(\mathbf{r}) \right\}. \end{aligned}$$

Here τ^a are the Pauli matrices, λ is the parameter employed to tune across the transition, and g is the Yukawa coupling between the fermions and bosons. We have included two sources of spatial randomness. The spatially random potential $v(\mathbf{r})$, with ensemble averages $v(\mathbf{r}) = 0$, $v(\mathbf{r})v(\mathbf{r}') = v^2 \delta(\mathbf{r} - \mathbf{r}')$, acts on the fermion density, and plays a central role in the theory of disorder-induced electron localization [8]. Such fermion localization effects are also present here, but all indications are that such effects are not important for the cuprates. Instead, our focus will be on the more relevant ‘Harris disorder’, induced

by spatial randomness in the position of the quantum critical point. Following Ref. [7], we have represented this by a spatially random Yukawa coupling $g'(\mathbf{r})$ with $g'(\mathbf{r}) = 0$, $g'(\mathbf{r})g'(\mathbf{r}') = g'^2 \delta(\mathbf{r} - \mathbf{r}')$. Such Harris disorder can lead to boson localization at low temperatures [2, 9], where it must be treated non-perturbatively, as we do below. But in higher temperature regimes, where the bosons do not localize, we can add a large number of flavor labels to the fields so that (S17) is amenable to a large flavor solution [6, 7, 10].

Patel *et al.* [9] have studied the YSYK model (S17) at $g = 0$ by large scale, high precision quantum Monte Carlo simulations (with no additional flavors), and their results for the imaginary time spin susceptibility appear in Fig. 4E of the main text. We describe below use the approach of Ref. [2] which treats the interactions in a mean-field manner, but accounts for disorder numerically exactly; this approach has the advantage of allowing exact analytic continuation to real frequencies at arbitrary temperatures. The results of Ref. [2] are in general agreement with the exact Monte Carlo results of Ref. [9]: both show an extended quantum Griffiths phase with ω/T scaling, but the value of α is smaller and more reliable in the Monte Carlo study.

The approach of Ref. [2] is to integrate out the fermions from (S17) (assuming fermionic eigenmodes remain extended), and consider the resulting Landau-damped Hertz-Millis theory for the boson ϕ alone. The spatial disorder in the Yukawa coupling $g'(\mathbf{r})$ will lead to disorder in all couplings in the effective boson theory. For simplicity, we retain only the most relevant ‘random mass’ disorder in the tuning parameter $\lambda \rightarrow \lambda + \delta\lambda(\mathbf{r})$. We also drop the longer-range RKKY couplings between the ϕ that will be induced by integrating out the fermions [11]. We discretize the boson theory on a lattice of sites (labeled by j), and write the SDW order parameters in terms of a real ϕ with a single index $a = 1 \dots M$ with $M = 12$. In this manner, we obtain the action

$$\begin{aligned} \mathcal{S} = & \mathcal{S}_\phi + \mathcal{S}_{\phi d} \\ \mathcal{S}_\phi = & \int d\tau \left[\frac{J}{2} \sum_{\langle ij \rangle} (\phi_{ia} - \phi_{ja})^2 + \right. \\ & \left. \sum_j \left\{ \frac{\lambda + \delta\lambda_j}{2} \phi_{ja}^2 + \frac{u}{4M} (\phi_{ja}^2)^2 \right\} \right] \\ \mathcal{S}_{\phi d} = & \frac{T}{2} \sum_{\Omega} \sum_j (\gamma|\Omega| + \Omega^2/c^2) |\phi_{ja}(i\Omega)|^2, \quad (\text{S18}) \end{aligned}$$

where Ω is a Matsubara frequency at a temperature T , γ is the Landau damping, and the Ω^2/c^2 term has been inserted as a high frequency cutoff. The random mass disorder satisfies $\delta\lambda(\mathbf{r}) = 0$, $\delta\lambda(\mathbf{r})\delta\lambda(\mathbf{r}') = \delta\lambda^2 \delta(\mathbf{r} - \mathbf{r}')$. For simplicity, we have assumed a global $O(M)$ symmetry, but this assumption can be relaxed without significantly modifying the results.

The theory in (S18) has been studied using a strong disorder renormalization group [12–14]. But the same basic results are obtained by the method of Ref. [2] (originally used for a related problem in $d = 1$ in Ref. [15]), which also allows study of the crossover at higher energies to weak disorder, and this will be important for our purposes. Following Refs. [2, 15], we replace \mathcal{S}_ϕ by an effective quadratic action, while renormalizing the space dependent mass in a self-consistent manner; this leads to

$$\begin{aligned} \tilde{\mathcal{S}}_\phi &= \int d\tau \left[\frac{J}{2} \sum_{\langle ij \rangle} (\phi_{ia} - \phi_{ja})^2 + \sum_j \frac{\tilde{\lambda}_j}{2} \phi_{ja}^2 \right] \\ \tilde{\lambda}_j &= \lambda + \delta\lambda_j + \frac{u}{M} \sum_a \langle \phi_{ja}^2 \rangle \tilde{s}_{\phi+S_{\phi d}} \\ &= \lambda + \delta\lambda_j + uT \sum_\Omega \sum_b \frac{\psi_{bi}\psi_{bj}}{\gamma|\Omega| + \Omega^2/c^2 + e_b}, \end{aligned} \quad (\text{S19})$$

where e_b and ψ_{bj} are eigenvalues and eigenfunctions of the ϕ quadratic form in $\tilde{\mathcal{S}}_\phi$, labeled by the index $b = 1 \dots L^2$ for a $L \times L$ sample. For each disorder realization δs_j , the values of $\tilde{\lambda}_j$ are determined by numerically solving (S19), and this also yields results for the eigenvalues e_b and the eigenvectors ψ_{bj} . The dynamic spin susceptibility is then computed at a real frequency ω from

$$\chi_{ij}(\omega) = \sum_b \frac{\psi_{bi}\psi_{bj}}{-i\gamma\omega - \omega^2/c^2 + e_b}, \quad (\text{S20})$$

followed by a Fourier transform from spatial co-ordinates to momenta.

Results from the computation above are presented in Fig. 4 of the main text, and Figs. S1-S9 below. The chosen parameter values are $J = 1$, $\gamma = 1$, $c^2 = 10$, $u = 1$ and $\delta\lambda^2 = 0.25$. The quantum critical point at $T = 0$ is at $\lambda_c = -0.4586$ [2]. We used a system size of 160×160 and averaged over 20 disorder realizations. We can set the energy scale by identifying the highest energy spin excitation ($c\sqrt{8J} \approx 9$ with the highest energy spin wave (≈ 300 meV [16]). This leads to the estimate $300/9 \approx 33$ meV as the unit of energy for the numerics.

The results for the dynamic spin susceptibility at the ordering wavevector \mathbf{Q}_δ were shown in Fig. 4 of the main text for $\lambda = \lambda_c$, where we found good ω/T scaling. Fig. S1 extends these results to $\lambda > \lambda_c$. Now we find ω/T scaling only for smaller values of ω/T . This restriction of ω/T scaling to $\omega \lesssim T$ for $\lambda > \lambda_c$ is not at odds with the experimental results in the main text, which also, strictly speaking, establish ω/T scaling for $\omega \lesssim T$ as the range of ω values available is not enough to achieve larger values of ω/T at the larger values of T that are considered.

The value of the exponent α decreases monotonically with increasing distance from the critical point (increasing λ). In Fig. S2, we show that using a smaller value of

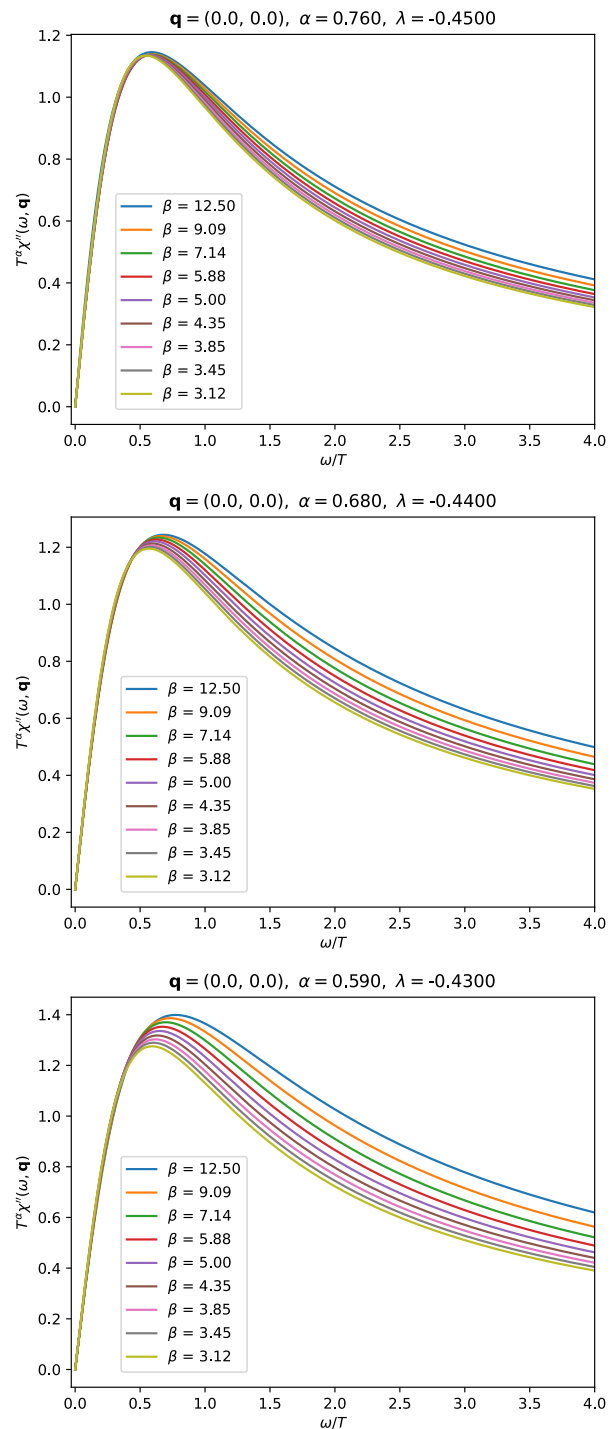


Fig. S1: **Scaling plots of the dynamic spin susceptibility at the ordering wavevector for $\lambda > \lambda_c = -0.4586$.** Results for $\lambda = \lambda_c$ are in Fig. 4B in the main text.

α makes little difference to the quality of the fit at small ω/T , which is the region at which scaling is established in the observations.

Fig. S3 shows similar results for the *local* dynamic spin

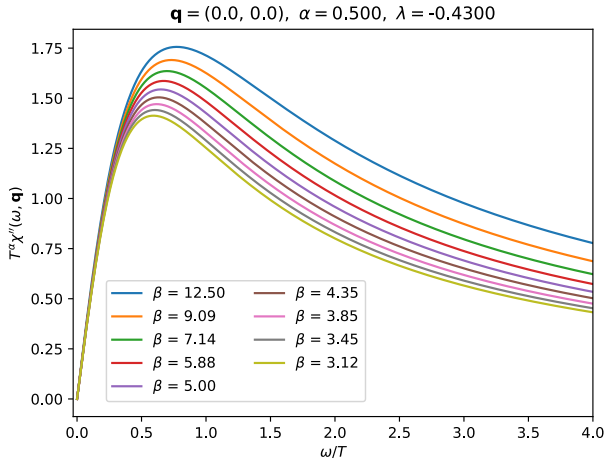


Fig. S2: **Scaling plots of the dynamic spin susceptibility at the ordering wavevector for $\lambda = -0.43$.** A smaller value of the exponent α is used in comparison to the corresponding plot in Fig. S1.

susceptibility

$$\chi_L''(\omega) = \int \frac{d^2\mathbf{q}}{4\pi^2} \chi''(\mathbf{q}, \omega) \quad (\text{S21})$$

for $\lambda \geq \lambda_c$. Now we find that ω/T scaling holds for all values λ , an indication that the criticality for $\lambda > \lambda_c$ is from localized spin fluctuations. This is just as expected from a quantum Griffiths critical phase. By scaling, the exponent for the local susceptibility $\alpha + \mu = 2/z$, and this is consistent with our values $\mu = 0.1$ to 0.16 , $\alpha = 0.84$ to 0.59 and $z = 2.1$ to 2.6 respectively for the range of $\lambda = -0.4586$ to -0.4300 considered.

Fig. S4 extends the analysis of scaling for the local and ordering wavevector susceptibilities at $\lambda = \lambda_c$ to much lower values of T , showing a breakdown of ω/T scaling at low T . This is consistent with results for the boson density of states in Ref. [9], which showed a crossover from the constant density of states associated with marginal Fermi liquid behavior at higher energy, to a regime dominated by Griffiths effects at lower energy. The breakdown of ω/T scaling here in the dynamic spin susceptibility likely arises from the enhanced boson density of states at smallest energies, and could possibly be captured by experiments at lower temperatures than the ones considered in this work.

Next, we turn to the behavior of the inverse correlation length, κ , defined by (6) in the main text (also (S12)), which we adapted to

$$\frac{\chi''(\mathbf{q}, \omega)}{\chi''(\mathbf{q} = 0, \omega)} = \frac{\kappa^4(\omega)}{[\kappa^2(\omega) + 4 - 2\cos(q_x) - 2\cos(q_y)]^2}. \quad (\text{S22})$$

Fig. S5 shows that (S22) provides an excellent fit to the numerical data, and this enables determination of

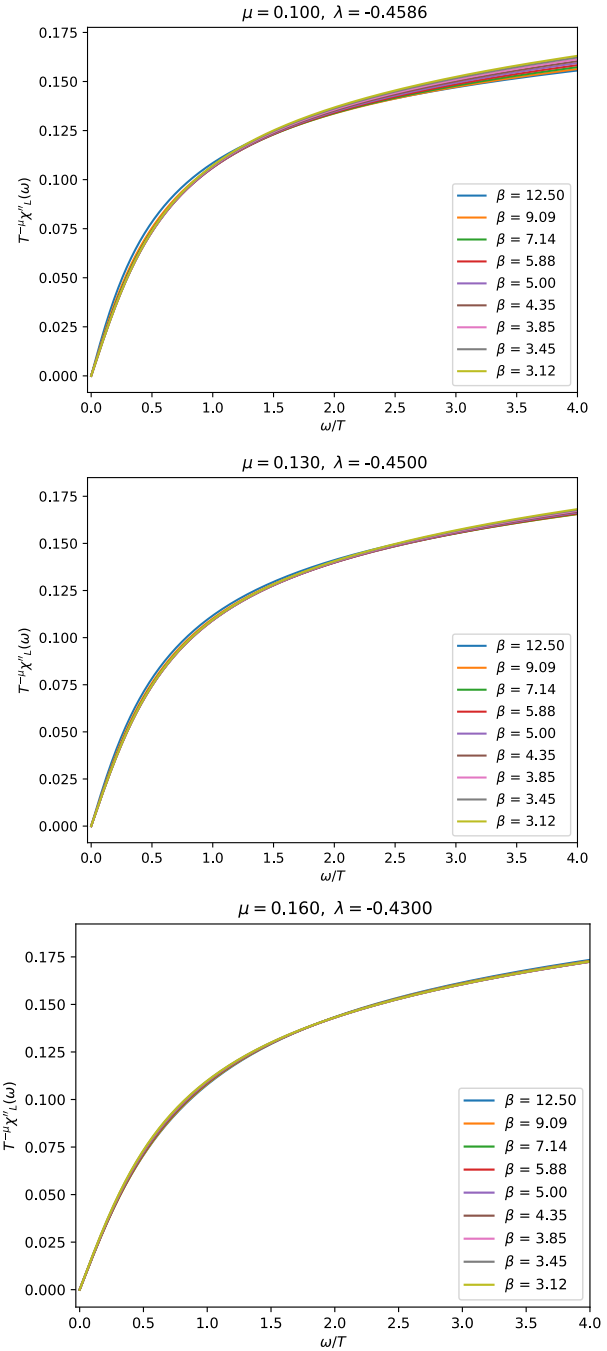


Fig. S3: **Scaling plots of the local dynamic spin susceptibility for $\lambda \geq \lambda_c = -0.4586$.**

$\kappa(\omega, T)$. Our results for κ and their scaling are shown in Fig. 4C,D of the main text at $\lambda = \lambda_c$. Corresponding results for $\lambda > \lambda_c$ appear in Figs. S6 and S7. As for the dynamics spin susceptibility at the ordering wavevector, ω/T scaling works for $\lambda = \lambda_c$, but only for smaller values of ω/T for $\lambda > \lambda_c$. The plots of Fig. S7 are shown on a logarithmic frequency scale in Fig. S8 (as in Figs. 3 and 4D of the main text), which exposes the lower frequency

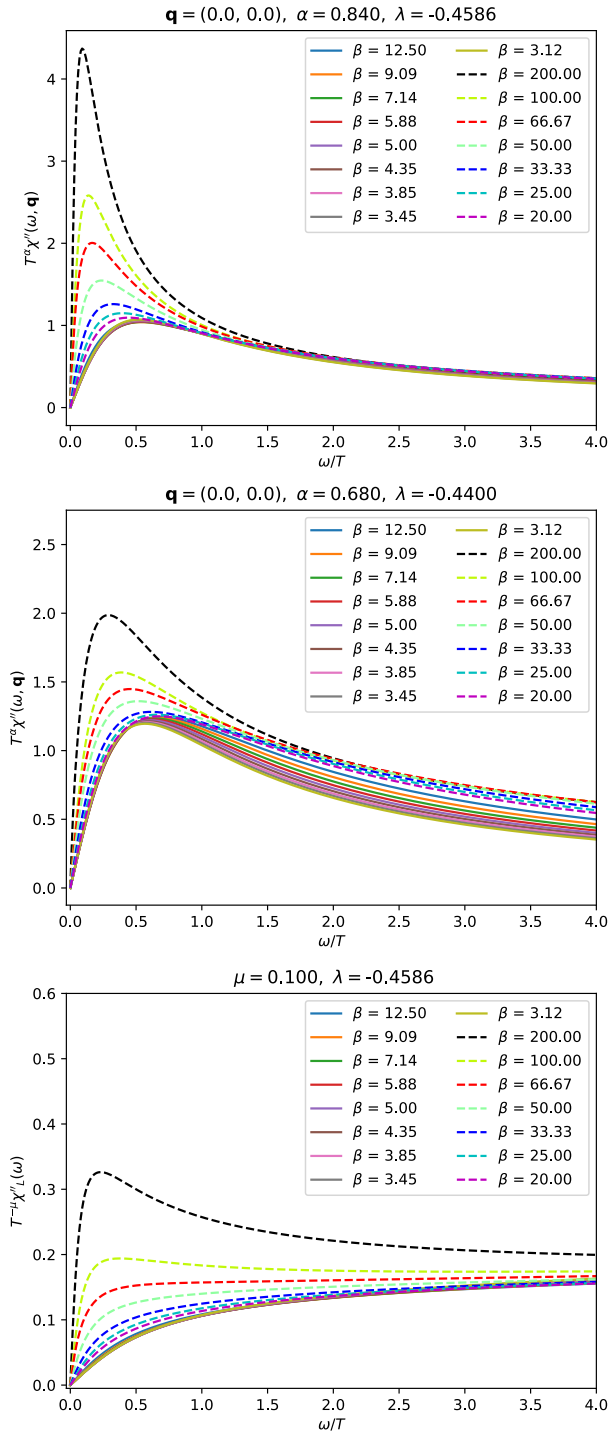


Fig. S4: **Breakdown of scaling at very low temperatures.** The dynamic susceptibilities at lower temperatures. Compare to the plots in Fig. 4 of the main text and Fig. S3.

range.

Finally, we complement plots of the resistivity induced by the disordered spin fluctuations in Fig. 4 of the main text at additional values of λ in Fig. S9. The resistivity

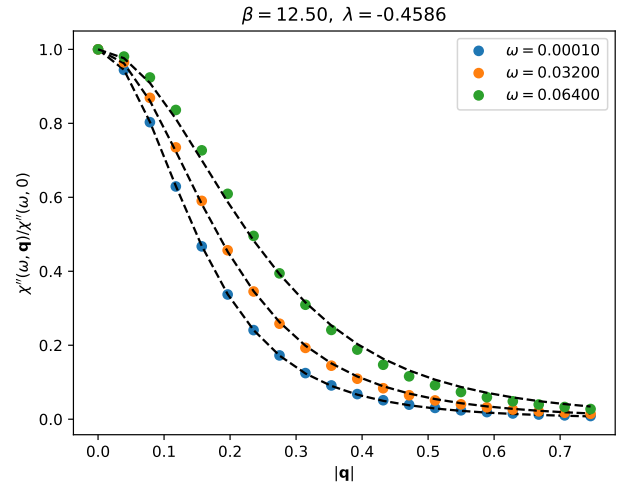


Fig. S5: Fits of the dynamic spin susceptibility to (6) in the main text, allowing determination of $\kappa(\omega, T)$.

was computed from the numerical results for $\chi''_L(\omega)$, as specified in Ref. [2].

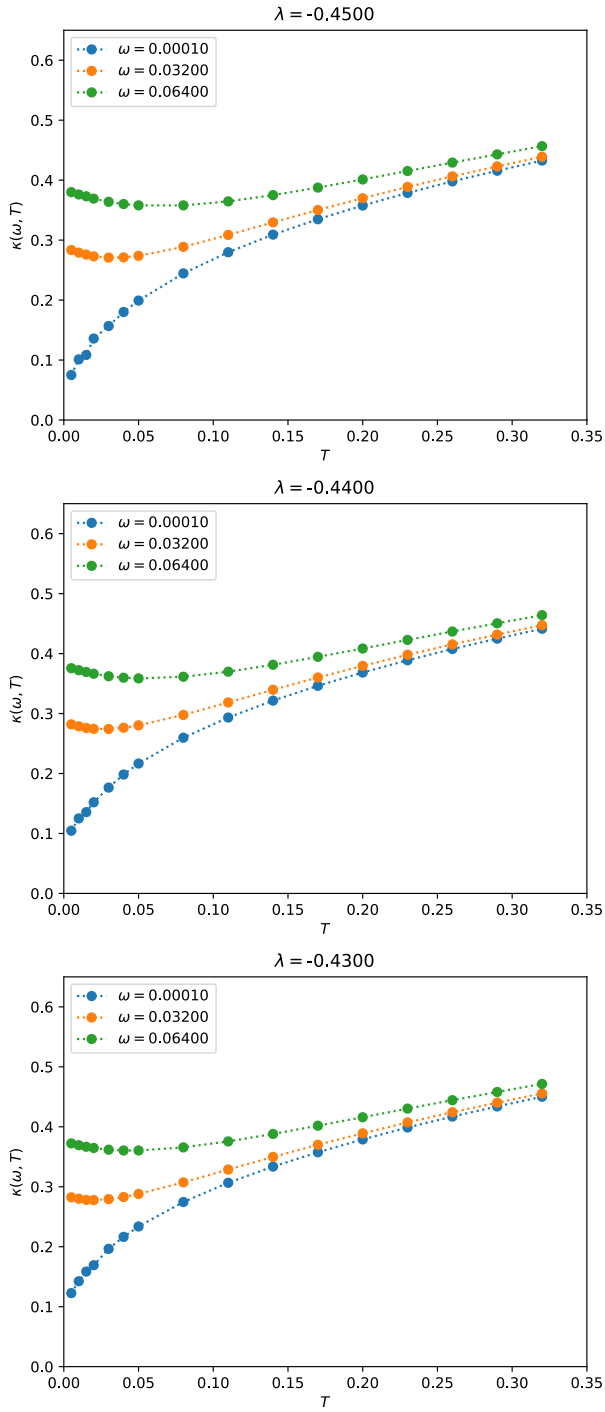


Fig. S6: Plots of κ for $\lambda > \lambda_c = -0.4586$. Results for $\lambda = \lambda_c$ are in Fig. 4C in the main text.

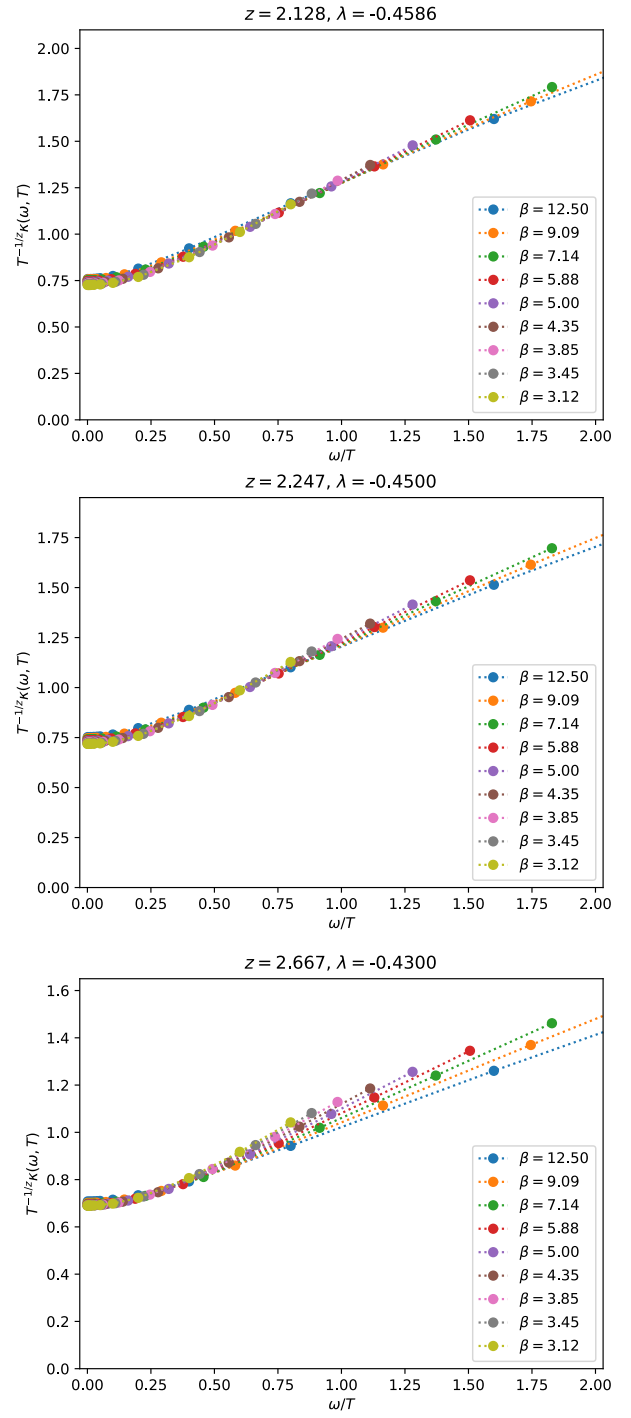


Fig. S7: Scaling plots of κ for $\lambda \geq \lambda_c = -0.4586$.

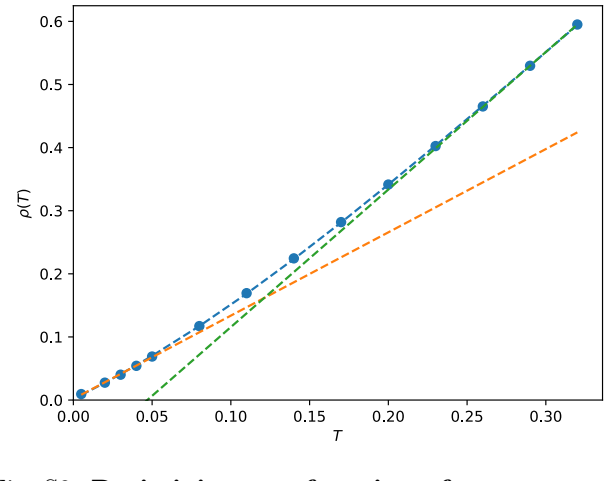
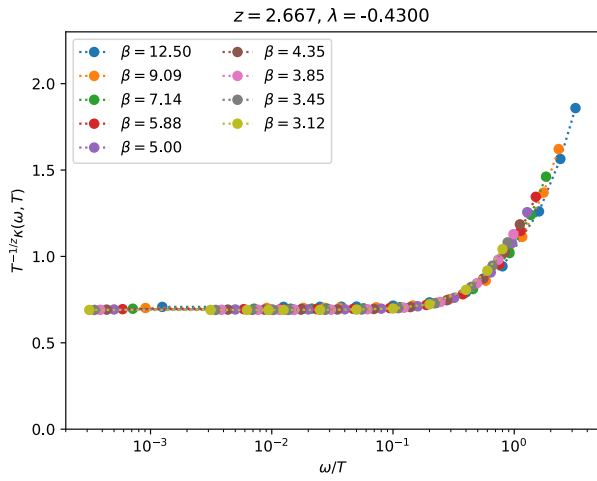
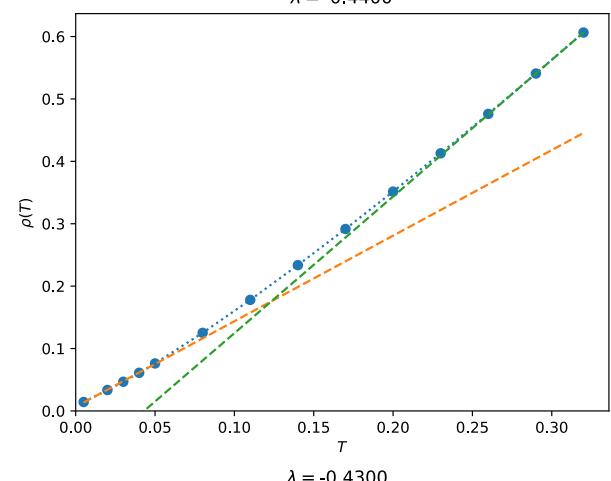
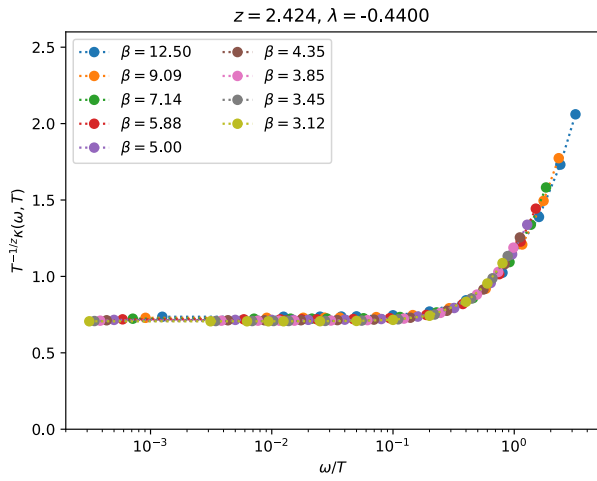
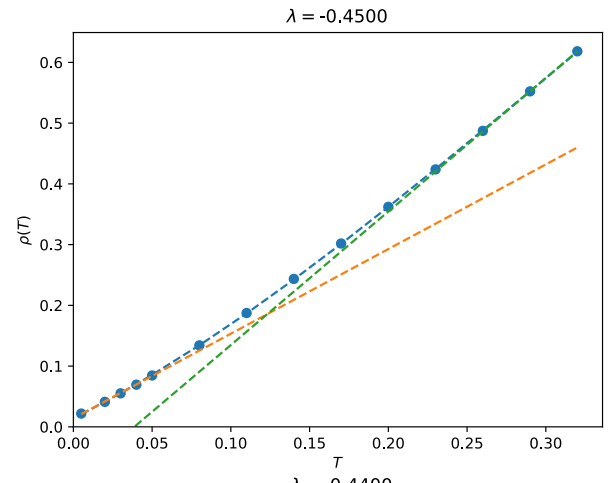
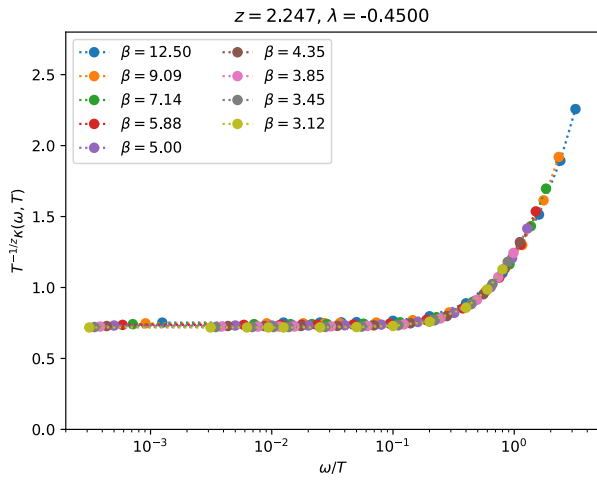


Fig. S8: **Scaling plots of κ for $\lambda > \lambda_c = -0.4586$.** As in Fig. S7, but with a logarithmic frequency axis. Compare to the experimental results in Figs. 3E and 4D of the main text.

Fig. S9: **Resistivity as a function of temperature.** As in Fig. 4F of the main text.

EXPERIMENTAL METHODS

Single-crystal sample growth and characterization

Single crystals of $\text{La}_{2-x}\text{Sr}_x\text{CuO}_x$ ($x = 0.22$) were grown by the travelling-solvent floating-zone method. The crystals were annealed in 1 bar of flowing oxygen at 800°C for six weeks. The Sr concentration was determined by scanning electron microscopy with electron probe micro-analyzer (SEM-EPMA) and inductively coupled plasma atomic emission spectroscopy (ICP-AES) to be $x = 0.215 \pm 0.005$. SQUID magnetometry measurements show that $T_{c,\text{onset}} = 26\text{K}$. The sample consists of 29.8g of LSCO crystal, mounted and co-aligned using the ALF single crystal diffractometer.

Inelastic neutron scattering

Inelastic neutron scattering measurements were performed at the LET direct time-of-flight spectrometer at ISIS. LET is a multiplexing instrument which allows for simultaneous collection of data at multiple neutron incident energies. Three fixed incident energies $E_i = 3.76, 6.82, 16.02$ meV were used for the whole data collection.

To this end, the sample was mounted with its c -axis vertical and the azimuthal angle swept over a range of $\sim 108^\circ$ about the region of interest. Measurements were taken at one degree intervals to ensure adequate coverage over the entire region around the $(1/2, 1/2)$ wavevector.

Two experiments were performed. In ‘Experiment 1’ we measure at 5 different temperatures including room temperature (290K) and the superconducting transition temperature (26K). In Experiment we measured at 3 of the 5 original temperatures with the sample rotated by 90° with respect to Experiment 1 and counted for a longer period at 300 K.

Data Analysis

The scattering cross-section is related to the scattering function $S(\mathbf{Q}, \omega)$ and energy- and wavevector-dependent magnetic response function $\chi''(\mathbf{Q}, \omega)$ by the fluctuation-dissipation theorem

$$\begin{aligned} \frac{k_i}{k_f} \frac{d^2\sigma}{d\Omega dE} &= S(\mathbf{Q}, \omega) \\ &= \frac{2(\gamma r_e)^2}{\pi g^2 \mu_B^2} |F(\mathbf{Q})|^2 \frac{\chi''(\mathbf{Q}, \omega)}{1 - \exp(-\hbar\omega/k_B T)}, \end{aligned} \quad (\text{S23})$$

where $(\gamma r_e)^2 = 0.2905$ barn sr^{-1} , and $F(\mathbf{Q})$ the magnetic form factor.

Counts measured at position sensitive detectors were normalized to a vanadium standard to correct for differ-

ences in detector efficiency and then used to reconstruct the momentum and energy-dependent scattering function $S(\mathbf{Q}, \omega)$. This process was repeated for each E_i producing three 4-D datasets at each temperature.

2-D \mathbf{Q} Slices

Our data analysis procedure involved generating 11 slices across the three E_i s over the energy range $\Delta E \sim 1-10$ meV. Data is binned over $L = \pm 1$ and $E = \hbar\omega \pm 0.5$ meV. The scattering function is converted to $\chi''(\mathbf{Q}, \omega)$ using Eqn. S23 following subtraction of a q -independent background. This background is determined through least-squares fitting (see section Cuts).

1-D \mathbf{Q} Cuts

In order to parameterise the excitations for a given ω, T , we use a further rebinning of the data slices. Two cuts through the high $|\mathbf{Q}|$ and low $|\mathbf{Q}|$ peaks, respectively at $\{(1/2, 1/2 - \delta), (1/2 - \delta, 1/2)\}$ and $\{(1/2, 1/2 + \delta), (1/2 + \delta, 1/2)\}$, are generated from each slice by binning along the \mathbf{Q} -direction perpendicular to the cut (see Fig. 1D in the main text).

Finally, we carry out a resolution-corrected least-squares fit (see Fig. S10) to each cut using the Tobyfit module in Horace [17]. The susceptibility is modelled by Eqn. S12. This has two energy-dependent parameters $\chi''(\mathbf{Q}_\delta, \omega)$ and $\kappa(\omega)$ which control the height and width of the peaks in \mathbf{Q} respectively. The incommensurability δ of the excitations also enters into the model via $R(\mathbf{Q})$.

The value of δ in Eqn. S13 was fixed for each temperature. The fitted values ranged from $\delta = 0.139$ to $\delta = 0.131$ for $T = 26$ and 300 K respectively. When making T -dependent (scaling) plots we evaluated the fitted $\chi''(\mathbf{Q}_\delta, \omega)$ for the $T = 26$ K value of δ . in the final fits but found to have a slight systematic decrease from $\delta = 0.139$ to $\delta = 0.131$ over the range 26K to 300K. This was determined by averaging over energy dependent best-fit values below 5meV where the peaks are sharp. We also fit a q -independent background in the model structure factor for each cut.

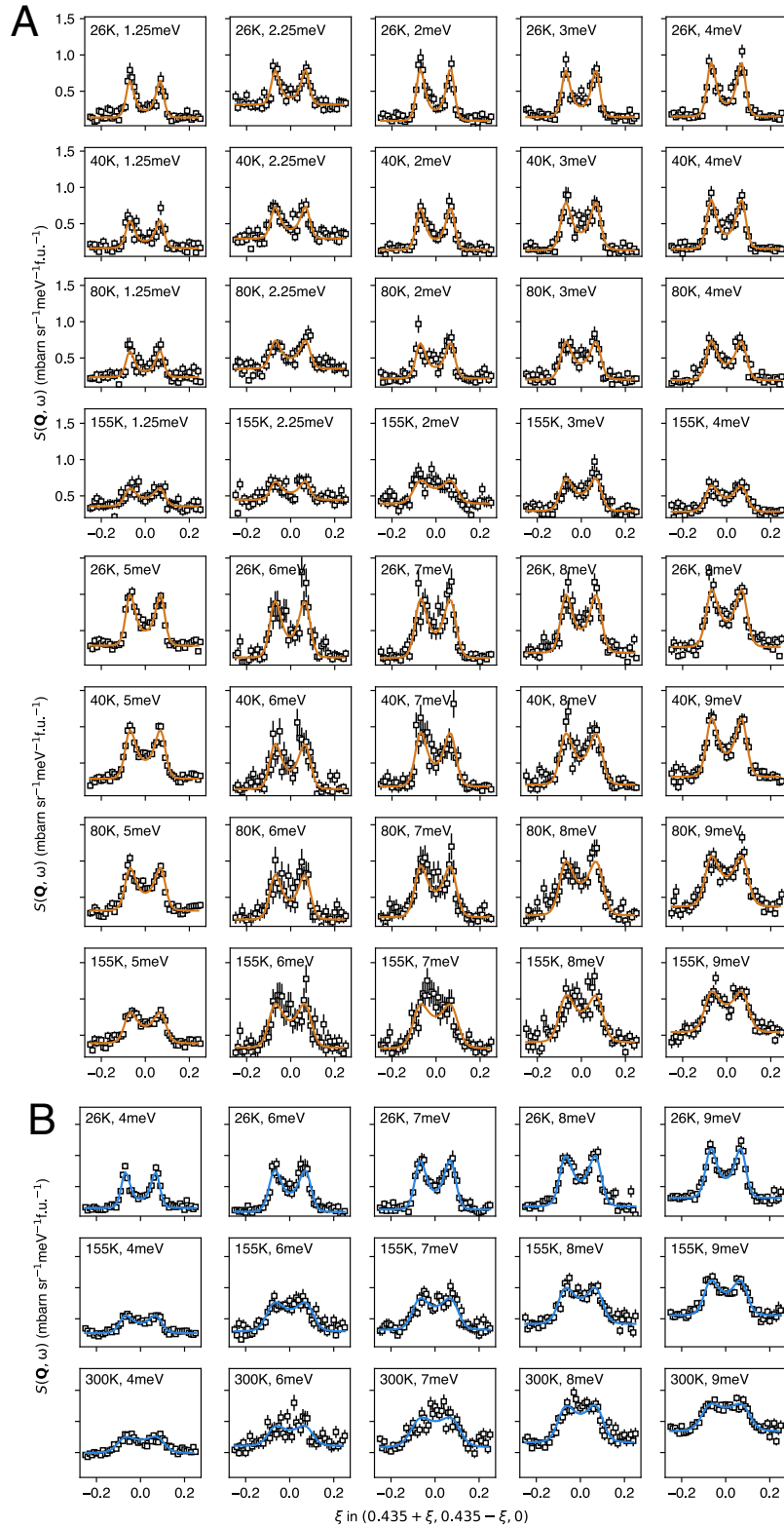


Fig. S10: A representative selection of $S(\mathbf{Q}, \omega)$ cuts and fits to the model described in the main text. **(A)** Experiment 1. **(B)** Experiment 2.

[2] A. A. Patel, P. Lunts, and S. Sachdev, Proceedings of the

[1] G. Aeppli, T. Mason, S. Hayden, H. Mook, and J. Kulda, Science **278**, 1432 (1997).

- National Academy of Sciences **121**, e2402052121 (2024).
- [3] S. Sachdev, “The foot, the fan, and the cuprate phase diagram: Fermi-volume-changing quantum phase transitions,” (2025), arXiv:2501.16417 [cond-mat.str-el].
 - [4] J. A. Hertz, Phys. Rev. B **14**, 1165 (1976).
 - [5] A. J. Millis, Phys. Rev. B **48**, 7183 (1993).
 - [6] I. Esterlis, H. Guo, A. A. Patel, and S. Sachdev, Phys. Rev. B **103**, 235129 (2021).
 - [7] A. A. Patel, H. Guo, I. Esterlis, and S. Sachdev, Science **381**, 790 (2023).
 - [8] P. A. Lee and T. V. Ramakrishnan, Rev. Mod. Phys. **57**, 287 (1985).
 - [9] A. A. Patel, P. Lunts, and M. S. Albergo, “Strange metals and planckian transport in a gapless phase from spatially random interactions,” (2024), arXiv:2410.05365 [cond-mat.str-el].
 - [10] C. Li, D. Valentinis, A. A. Patel, H. Guo, J. Schmalian, S. Sachdev, and I. Esterlis, Phys. Rev. Lett. **133**, 186502 (2024).
 - [11] J. H. Van Vleck, Rev. Mod. Phys. **34**, 681 (1962).
 - [12] J. A. Hoyos, C. Kotabage, and T. Vojta, Phys. Rev. Lett. **99**, 230601 (2007).
 - [13] T. Vojta, C. Kotabage, and J. A. Hoyos, Phys. Rev. B **79**, 024401 (2009).
 - [14] T. Vojta, in *Lectures on the Physics of Strongly Correlated Systems XVII: Seventeenth Training Course in the Physics of Strongly Correlated Systems*, American Institute of Physics Conference Series, Vol. 1550, edited by A. Avella and F. Mancini (AIP, 2013) pp. 188–247, arXiv:1301.7746 [cond-mat.dis-nn].
 - [15] A. Del Maestro, B. Rosenow, M. Müller, and S. Sachdev, Phys. Rev. Lett. **101**, 035701 (2008).
 - [16] S. M. Hayden, G. Aeppli, R. Osborn, A. D. Taylor, T. G. Perring, S. W. Cheong, and Z. Fisk, Phys. Rev. Lett. **67**, 3622 (1991).
 - [17] R. Ewings, A. Buts, M. Le, J. van Duijn, I. Bustinduy, and T. Perring, Nuclear Instruments and Methods in Physics Research Section A: Accelerators, Spectrometers, Detectors and Associated Equipment **834**, 132 (2016).